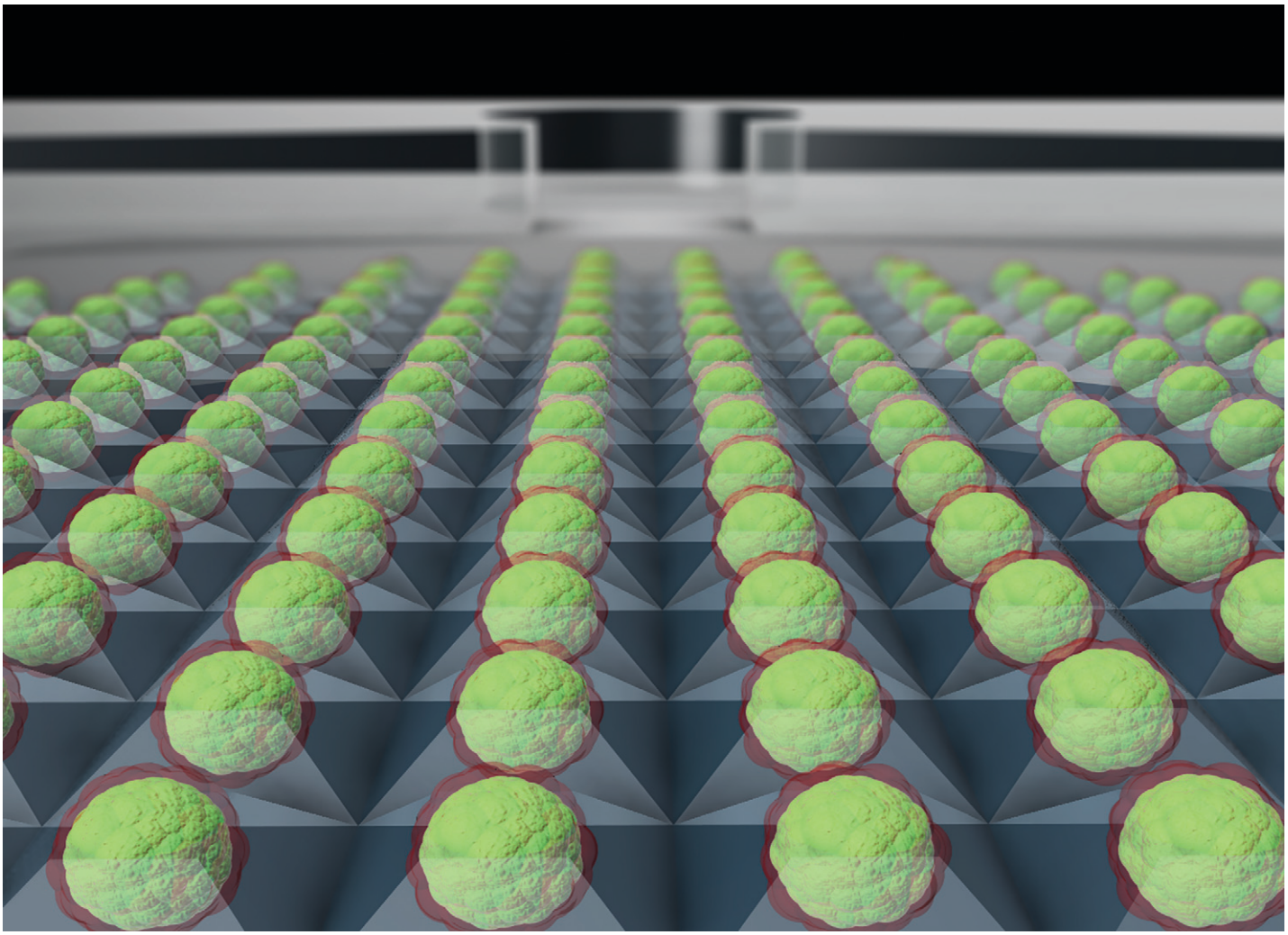

Showcasing research on high-throughput drug screening platform with multilayered spheroid from Professor Junmin Lee's laboratory, Department of Materials Science and Engineering, Pohang University of Science and technology (POSTECH), Korea.

High throughput drug screening platform utilizing capillary and artery cell layered models based on tumor–vascular cell interactions

We developed a Tumor model surrounded by vascular cells to better mimic the tumor microenvironment. By encapsulating these models in hydrogels and applying media circulation, we recreated key features like cell-cell and cell-matrix interactions and shear stress. This dynamic system enables high-throughput screening (HTS) for anti-cancer drugs, supporting cancer treatment research and development.

Image reproduced by permission of Jihyeon Song and Yeji Lee from *Lab Chip*, 2025, **25**, 2349.

As featured in:

See Junmin Lee, Han-Jun Kim *et al.*, *Lab Chip*, 2025, **25**, 2349.

ROYAL SOCIETY OF CHEMISTRY

rsc.li/loc

Registered charity number: 207890

Lab on a Chip

PAPER

View Article Online
View Journal | View Issue

Cite this: *Lab Chip*, 2025, **25**, 2349

High throughput drug screening platform utilizing capillary and artery cell layered models based on tumor–vascular cell interactions†

Jihyeon Song, ‡[a] Yeji Lee, ‡[a] Min-Seok Kim, [b] Giheon Ha, [a] WonJun Jang, [bc] Ulziituya Batjargal, [bc] Younggyun Kim, [d] Han-Jun Kim *[bc] and Junmin Lee *[a]

Interactions between tumors and adjacent blood vessels are critical in the tumor microenvironment (TME) for influencing angiogenesis and hematogenous metastasis. Understanding these interactions within the native TME is vital for targeting various tumors, including brain tumors, due to the complexities of the blood–brain barrier. Developing an accurate tumor model that includes cell–cell and cell–matrix interactions, as well as blood flow-induced shear stress, is essential for high-throughput screening (HTS) of anti-cancer drugs. Here, we developed a glioblastoma (GBM) model surrounded by vascular cells. The arterial model was constructed by encapsulating GBM spheroids with layers of human smooth muscle cells (SMCs) and human umbilical vein endothelial cells (HUVECs), while the capillary cell layered model used only HUVECs. Comparative analysis with tumors from different organs revealed the significant role for platelet endothelial cell adhesion molecule (PECAM) in GBM–blood vascular cell interactions. Cytokine secretion analysis demonstrated PECAM's impact on tumor-specific angiogenic potential. Testing with anti-cancer drugs revealed increased expression of PECAM-associated proteins, drug resistance cytokines, and genes associated with tumor progression and metastasis. Additionally, we developed a HTS platform by encapsulating these tumor models in hydrogels and subjecting them to media circulation, effectively mimicking the dynamic TME, suitable for cancer treatment research and drug development.

Received 13th November 2024,
Accepted 26th March 2025

DOI: 10.1039/d4lc00950a

rsc.li/loc

1. Introduction

Blood vessels are tubular structures responsible for the circulation of blood throughout the body. They play crucial roles in regulating hemodynamic processes, facilitating fluid filtration, contributing to immune modulation, and various other physiological functions.[1] The interaction between tumors and adjacent capillaries and arteries holds significant importance in the context of the tumor microenvironment (TME).[2] For example, tumor angiogenesis and hematogenous metastasis represent pivotal features of tumor progression, occurring through intricate interactions with blood vessels.[3] Furthermore, in the case of brain tumors, understanding of blood–brain-barrier is particularly vital for targeting brain tumors.[4,5] Exploring interactions between tumors and blood vessels, including capillaries and arteries in the native TME, is essential, because (i) native tumor phenotypes interacting with various cells in blood vessels may differ from those in conventional artificial tumor spheroid models, (ii) endothelial cell junctions' adherences and tightness could be influenced by tumors *via* cell–cell interactions,[6] and (iii) anticancer-drugs delivered through the vasculature to tumors differ from conventional drug screening methods that directly expose cancer cells or tumor spheroids to the drugs. Despite this, limited effort has been made to develop a high-throughput tumor model incorporating blood vessels for studying tumor–vascular cell interactions and screening various anticancer drugs.[7–9]

Endothelial cells in vessels possess multiple junctions, including adherens and tight junctions, which are crucial for their regulatory functions. Adherens junctions establish and maintain cell–cell adhesion, remodel the actin cytoskeleton, and regulate transcription.[10] Regulation of vascular endothelial cadherin (VE-cadherin) leads to variations in endothelial barrier functions and endothelial cell lineages, affecting the expression of claudin-5.[11] The expression levels of platelet endothelial cell adhesion molecule (PECAM) indicate different

[a] *Department of Materials Science and Engineering, Pohang University of Science and Technology (POSTECH), Pohang 790-784, Republic of Korea. E-mail: junmin@postech.ac.kr*
[b] *College of Pharmacy, Korea University, Sejong, 30019, Republic of Korea. E-mail: hanjun@korea.ac.kr*
[c] *Interdisciplinary Major Program in Innovative Pharmaceutical Sciences, Korea University, Sejong 30019, Republic of Korea*
[d] *Department of Bioengineering, University of Southern California, Los Angeles, CA 90089, USA*

† Electronic supplementary information (ESI) available. See DOI: https://doi.org/10.1039/d4lc00950a

‡ These authors equally contributed to this work.

stages of intercellular adhesions and steady-state barrier functions.[12] Tight junctions, maintained by proteins such as claudins and occludins, are essential for endothelial cells to form a strong barrier and regulate monolayer permeability.[10] The TME can regulate the expression level of these junction proteins in endothelial cells, which may influence the susceptibility of tumors to anticancer drugs.[13–15] Therefore, developing tumor models that incorporate surrounding capillaries and arteries is essential to investigate how tumor–vascular cell interactions influence the modulation of adherens and tight junctions in endothelial cells.

To understand how cancer interacts with surrounding vascular endothelial cells, the expression of junction proteins for endothelial cells is a crucial parameter indicative of vessel layer maturation. To test this hypothesis, we developed a miniature tumor model that incorporates vessels replicating the native TME structures. i) Capillary cell layered model: patient-derived tumor spheroids were used to fabricate capillary cell layered models by encapsulating them with endothelial cells. ii) Artery cell layered model: the tumor spheroids were encapsulated with smooth muscle cells (SMCs) followed by endothelial cells to mimic native artery layers. This configuration allows gradual delivery of oxygen and nutrients from the periphery to the core, simulating the hypoxic gradient in the native TME. Analysis of endothelial cell junction marker expression revealed the impact of tumor presence on blood vessel maturation. Genome analysis of tumor–vessel models demonstrated different levels of tumor progression and metastasis markers compared to tumor-only models. Using a high-throughput screening (HTS) platform built with these tumor–vessel models, we identified drug-resistance profiles, validating the proposed HTS model as a potential drug screening platform for personalized medicine. Furthermore, interactions of SMCs and HUVECs, as well as between human mesenchymal stem cells (hMSCs) and HUVECs, were investigated to demonstrate the role of hMSCs in differentiating into pericytes and enhancing endothelial junction maturation.

2. Methods

2.1. Materials

All reagents and chemicals were obtained from Sigma-Aldrich, unless stated otherwise. Cell culture plastics were obtained from SPL life sciences. Cell culture reagents and media were obtained from Gibco. Mouse anti-VE-cadherin (sc-9989), and anti-PECAM (sc-376764) were purchased from ABclonal. Rabbit anti-CLDN5 (A10207), and anti-occludin (A2601) were purchased from Santa Cruz Biotechnology. Alexa Fluor 488 conjugated goat anti-rabbit antibody (A11008), Alexa Fluor 647 conjugated goat anti-mouse antibody (A21235), and DAPI (D1306) were purchased from Invitrogen.

2.2. Cell culture

Eight cell types were used in this project: MSC (PCS-500-012), SMC (PCS-100-012), HUVEC (PCS-100-010), GBM (SNU-1105), breast cancer (SK-BR-3), liver cancer (SNU-182), pancreas cancer (Capan-2), and lung cancer (A549). MSC, SMC, and HUVEC were purchased from ATCC. All the cancer cells including GBM was purchased from the Korean Cell Line Bank at Seoul National University. All cells were cultured in T175 flasks and maintained in a humidified incubator at 37 °C and 5% CO_2. SMC and GBM were cultured in the Dulbecco's modified Eagle medium (DMEM) (Gibco 11965-092, Invitrogen Co., USA) supplemented with 10% v/v fetal bovine serum (35-015-CV, Corning) and 1% penicillin–streptomycin–glutamine (PSG) (Gibco, 10378-016). We added 50 μl recombinant human FGF basic/FGF2/bFGF (146 aa) protein (FGF) (bio-techne, 233-FB/CF) per 50 ml SMCs culture media. MSC was cultured in low glucose Dulbecco's modified Eagle medium (DMEM-lg) (Gibco, 11885-084) supplemented with 10% v/v fetal bovine serum and 1% penicillin–streptomycin–glutamine. We added 50 μl of FGF per 50 ml of MSC culture media. HUVEC medium was composed of Endothelial Cell Growth Medium 2 (Promo Cell, C-22022) and supplemented with Endothelial Cell Growth Medium MV 2 SupplementMix (Promo Cell, C-39226) and 1% penicillin–streptomycin–glutamine. Media was warmed for 30 minutes in a 37 °C water bath before replacement. The media was replaced every four days. Cells were passaged at nearly 90% confluence using 0.25% trypsin–EDTA (Gibco, 25200-056). Only HUVEC trypsinized with 0.05% trypsin solution of 0.25% trypsin–EDTA diluted with PBS in a 1 : 4 ratio. All cells were maintained below 90% confluency and only cell with passage numbers between 4 and 10 were used in this study.

2.3. Core cell culture for spheroid formation

All spheroids were formed in microwells where each well of the culture plate (Stem Cell Technologies, AggreWell™400, 24-well plates) had 1200 inverted pyramid-shaped microwells, each with a diameter of 400 μm. Single cells were seeded in these microwells following the protocol from Stem Cell Technologies. 500 μL of anti-adherence rinsing solution (Stem Cell Technologies, 07010) was pipetted into each of the 24-well plates. The plate was centrifuged (3000 rpm, 10 min) and washed with PBS. Cells were trypsinized from culture flasks, counted, and seeded into the microwells. Spheroids were maintained in a humidified incubator at 37 °C and 5% CO_2. Medium was changed every four days.

2.4. HUVEC cell layer seeding and culture

HUVECs were seeded on the 8th day of core spheroid culture, trypsinizing and counting the number of cells prior to the seeding process. After removing 1 ml of the existing media using a micropipette, 1 ml of media containing the number of HUVECs suitable for each condition was added for seeding. Spheroids were maintained in a humidified incubator at 37 °C and 5% CO_2. Medium was changed every four days.

2.5. Cell tracking in spheroids

Two different cell trackers, CMFDA (Invitrogen, CellTracker Green C2925) and CMAC (Invitrogen, CellTracker Blue, C2110) were used to observe the location of core spheroid cells and HUVECs, respectively. Both cell trackers had identical protocols from the manufacturers. First, a stock solution was prepared by dissolving cell trackers in DMSO at a stock concentration of 10 mM. Working solutions were then made by diluting stock solution 1000× in phosphate buffered saline (PBS). Cells were trypsinized from cell culture flasks and incubated in the working solution for 30 min at 37 °C. Cells were then centrifuged, and the working solution was removed. Cells were resuspended in fresh medium subsequently. These cells, labeled with the fluorescence dyes, were seeded onto the inverse pyramidal microwells. After spheroid formation, spheroids were visualized using a confocal microscope (STELLARIS 5, Leica).

All processes were performed out of direct lighting, and the samples were shielded from light using foil.

2.6. Immunofluorescence

Spheroids were fixed in 4% paraformaldehyde (Sigma) for 40 min and permeabilized in 0.1% Triton X-100 (Fisher) in PBS for 1 h. 1% bovine serum albumin (BSA) was employed to block the cells for 1 h. All these steps were performed at room temperature. The primary antibody labelling was performed in 1% BSA in PBS for overnight at 4 °C, followed by rinsing with PBS two times. The samples were treated with PBS containing 1% BSA and 2% goat serum for 30 min. Secondary antibody, and DAPI was performed in 2% goat serum, 1% BSA in PBS for 20 min in a humidified incubator (5% CO_2 and 37 °C). All antibody used in 1 : 250, and DAPI in 1 : 2500.

2.7. Human cytokine array

The cytokines in the conditioned cell culture media were assessed utilizing the Proteome Profiler™ human cytokines array kit (R&D Systems, ARY005B). Initially, the nitrocellulose membrane printed with 36 different capture antibodies was blocked with a blocking buffer for 1 hour at room temperature. Following this, a mixture comprising the cell culture media and antibodies was applied onto the membrane and left to incubate overnight at 4 °C on a shaker. Subsequent to multiple washes, the membranes underwent a 30 minute incubation with streptavidin-horseradish, followed by treatment with chemiluminescence detection reagents. Chemiluminescence blot detection was conducted using Amersham™ Image Quant™ 800 (Cytiva). The acquired dot blot image was subjected to quantitative analysis using Image J software. To quantify protein expression, a reference mask was applied to define the dot blot regions, and integrated density was measured. Each cytokine dot was duplicated, and the average intensity of the two spots was used for analysis. Reference spots consisted of three pairs (six dots in total), and their mean intensity was calculated for normalization. Background noise was determined by averaging the intensity of two negative control dots. The final relative expression value was obtained by subtracting the background signal from each dot and normalizing it to the mean intensity of the reference spots.

2.8. qRT-PCR

Samples for PCR were collected by floating the spheroids in AggreWell and centrifuged. After resuspension in PBS and washing by centrifugation, the remaining solution was removed, and the sample was prepared by freezing only the cells at −80 °C. According to the manufacturer's instructions, total RNA was extracted using the NucleoSpin RNA Plus RNA extraction kit from Macherey-Nagel (USA). This extracted RNA was then utilized to synthesize cDNA using the ReverTra Ace qPCR RT Kit from Toyobo (Japan). Real-time PCR was carried out for 45 cycles with the Thunderbird Next SYBR qPCR Mix from Toyobo. The real-time PCR amplifications were conducted for 5 s at 95 °C and 30 s at 60 °C for 45 cycles after the initial denaturation step of 30 s at 95 °C (Bio-Rad, CFX-384 platform). The primers were categorized into oncogene, tumor suppressor, Rho, and metastasis-related gene (see Table S1 in the ESI†). The average values of glyceraldehyde 3-phosphate dehydrogenase (GAPDH), beta-actin (β-actin), and 18s ribosomal RNA (18s rRNA) were validated and used as reference genes. GBM or GBM + HUVEC(Cap) were used as the control, and the results were expressed as fold change in threshold cycle (Ct) using the 2-ΔΔCT method. Heatmaps for the mRNA expression level results were created with the online tool Morpheus (USA, **https://software.broadinstitute.org/morpheus**).

2.9. Anti-cancer drug test

Doxorubicin hydrochloride (MERCK, PHR1789) and bevacizumab (Celechem, A2006) were used for drug testing. GBM spheroids were incubated for 7 days and capillary cell layered model spheroids for 21 days before being replaced with drug-containing media. For doxorubicin, the appropriate concentration (1 μM, 5 μM) was selected after testing the concentration-dependent cell viability, and bevacizumab was fixed at a concentration of 168 nM based on previous study.[16] The drug media was changed every 24 hours.[16] The drug media was changed every 24 hours. The cytotoxicity of the drugs was assessed by cell viability on days 1 and 2.

2.10. Device simulation

In this computational fluid dynamics (CFD) study using Fluent 2023 R1 (Ansys Inc.), by solving the governing equations (continuity and Navier–Stokes) of fluid motion within microfluidic device. 10% FBS DMEM, with a density of 1009 kg m^{-3} and a viscosity of 0.930 mPa s.[17] and is treated as an incompressible, homogeneous, Newtonian fluid. Laminar model is utilized to implement flow's viscous model, confirmed by Reynolds number.

Boundary conditions are considered as follows: a velocity of inlet with flow rates of 10 μL min^{-1} and atmospheric pressure is applied at outlet. The cross-sectional areas of both

the inlet and outlet are assumed to have dimensions of 0.45 μm by 0.45 μm, and no-slip conditions are enforced at the device walls. To solve the governing equations, the microfluidic device is discretized using a refined mesh to obtain more accurate velocity and wall shear stress solution. This simulation provides sufficient insights to appropriately achieve the mechanical environment of *in vivo* blood flow in a microfluidic device.

2.11. Image collection, processing, and analysis

Photographs of spheroids in the inverse pyramidal microwells were obtained using a confocal microscope (Leica). The characterization of spheroid shape (diameter, circularity, and aspect ratio) was performed using ImageJ through its pixel to micrometer conversion scale (Fiji).

Immunofluorescence images were also obtained using a confocal microscope (Leica). ImageJ was also used for the quantification of images collected. Spheroids were imaged for each condition and their fluorescence intensities were used to compare the expression of markers. Where adjustments were made to images these were performed on the entire image.

2.12. Statistical analysis

For morphology and intensity analysis, images were used without any preprocessing. Data were obtained from three

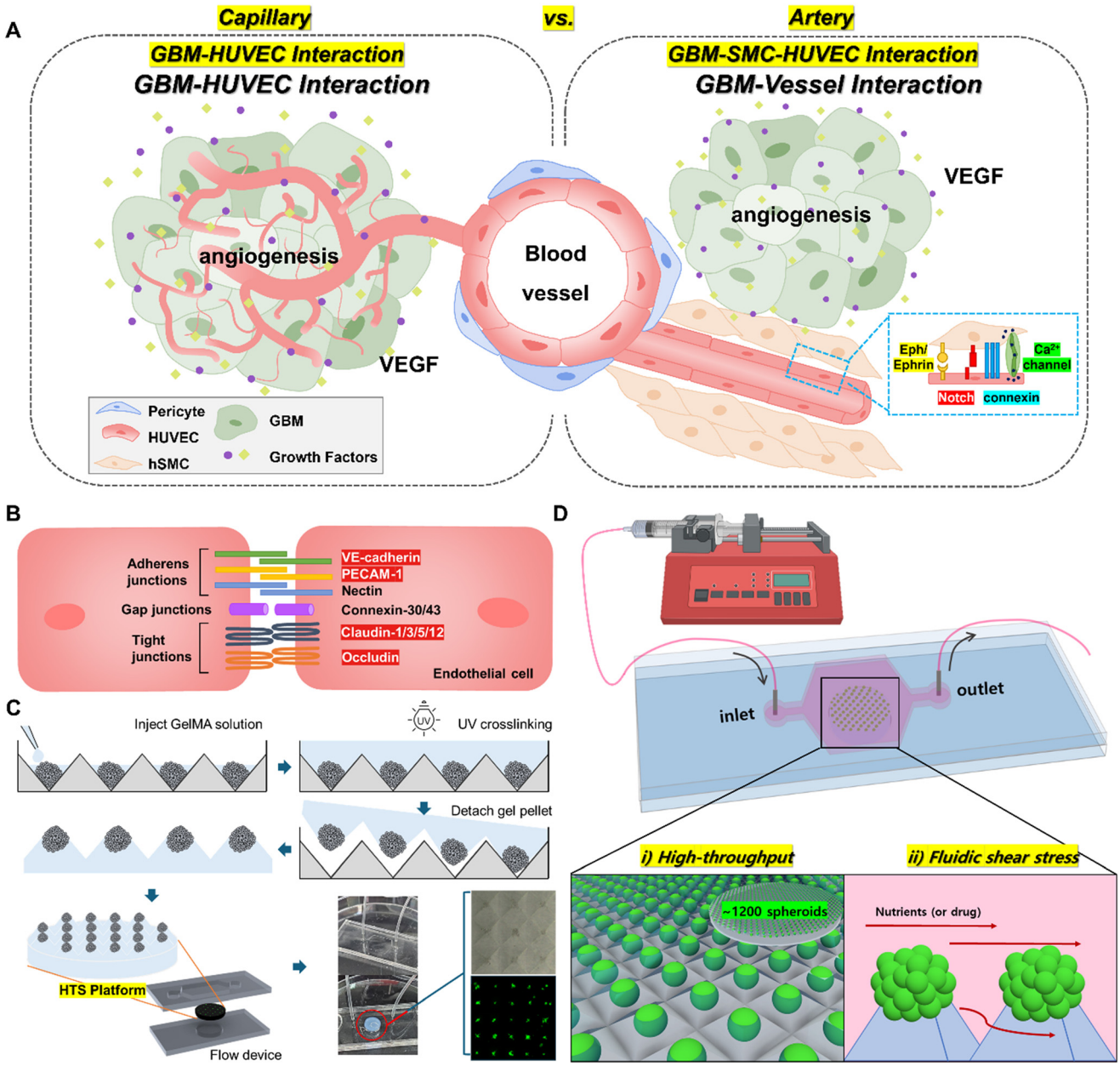

Fig. 1 Scheme for modeling arteries and capillaries. (A) Comparison of capillary and artery environments in the brain. (B) Scheme image of an endothelial intercellular junctions. (C) Schemes showing the fabrication strategy for high-throughput screening (HTS) platform using spheroids. (D) A schematic displaying the overview and features of flow device with HTS platform.

replicates and confirmed by at least three independent experiments. Mean ± standard deviation was used for presenting all data. One-way ANOVA with Tukey HSD (honestly significant difference) *post hoc* test was achieved in the statistical analyses. Statistics with a value of $p < 0.05$ were considered significant (****$p < 0.0001$; ***$p < 0.001$; **$p < 0.01$; *$p < 0.05$).

3. Results and discussion

3.1. Tumors actively interact with blood vessels

For high-throughput applications, it is essential to create miniaturized models that mimic the properties of native tissues. In the body, there are vessel-neighbor cells around blood vessels and tumors adjacent to them. Cancer and the surrounding blood vessels interact directly and indirectly through proteins, ion channels, and factors such as vascular endothelial growth factor (VEGF) (Fig. 1A). The method of studying cancer–vessel interaction by inserting cancer cells and HUVECs into polydimethylsiloxane (PDMS) devices is widely used, but there are limitations in directly interacting by inserting surrounding cells.[18–20] In this study, we developed microwell-based tumor spheroid surrounded by cells that constitute arteries and capillaries which can induce direct cancer–vessel interactions through the layering of endothelial and smooth muscle cells around the spheroids (for simplicity, the capillary cell layered model and artery cell layered model will be referred to as the capillary model and artery model hereafter). We developed the model by turning the actual environment inside out; the artery model has a layer of smooth muscle cells and vein endothelial cells, while the capillaries have only a vein endothelial cell layer encapsulating a tumor spheroid. Endothelial cells in spheroids interact themselves through junctions, such as adherens, gap, and tight junctions. Among them, adherens and tight junctions were chosen to evaluate endothelial cell functionality in the presence of cancer, since these junctions involved in cell permeability by controlling intercellular adhesion (Fig. 1B).[21–23] Through analysis of junction marker expression of endothelial cells, we could explore how the cancer cell–vascular cell interactions affect the connections between endothelial cells. In addition, we developed a high-throughput screening (HTS) platform capable of positioning numerous tumor spheroids at regular intervals within a hydrogel. Initially, tumor spheroids of uniform size were created within AggreWell plates. These AggreWell with spheroids were filled with a hydrogel prepolymer solution and then cured under UV-light to form the hydrogel-based tumor model (Fig. 1C). This model was subsequently loaded into an organ-on-a-chip system that allows for media flow applying shear stress to endothelial cells encapsulating tumors, thus establishing the HTS platform. This platform facilitates long-term culture of tumors and enables drug delivery and screening through flow conditions (Fig. 1D). The system has the advantage of being applied as a HTS manner and is considered biomimetic because it can be subjected to shear stress to endothelial cells in both capillary and artery models caused by the flow of media (Fig. 1D). In addition, because drugs or nutrients are delivered through the blood vessel endothelial cells rather than directly to the cancer, drug screening for tumors could be conducted in an environment that mimics the native environment where drugs travel through the bloodstream, follows the blood vessels, and passes through the vessel walls to reach the tumor. This platform could help in understanding the interactions of tumor–blood vessels as well as junctional interactions between endothelial cells within the vessels.

3.2. Cancer–capillary model spheroid formation and their shape analysis

GBM is a type of solid tumor and one of the most common and aggressive malignant tumors in the brain. Solid tumors are masses of cells that clump together and trigger angiogenesis to establish a blood supply essential for their growth and progression (Fig. 2A). The spheroid-based model provides (i) high cell–cell interactions, (ii) co-culture of multiple cells, and (iii) oxygen, nutrition, and pH gradient so that could mimic the native tumor microenvironment. To build a short-term evaluation *in vitro* system, we used inverted pyramidal microwells (400 um diameter) to generate GBM spheroids surrounded by HUVECs (Fig. 2C). To create a tumor–capillary model, core spheroids were initially created using only GBM. After 8 days, additional HUVECs were then seeded to form a HUVEC layer, resulting in a multilayer spheroid (Fig. 2B and C). GBMs were labeled with green cell trackers to visualize the formation of spheroid and then cultured for 7 days in 0%, 1%, and 10% FBS culture medium to determine the culture medium conditions favorable for spheroid formation (Fig. 2D). The decreasing diameter of the spheroids over time in all three concentration conditions indicates that the cells aggregate well into spheroid forms (Fig. 2E). Since spheroids need a medium with sufficient nutrients for a long-term culture, a medium condition with FBS was chosen; in the medium containing 10% FBS, approximately 20% of the spheroids escaped from the wells, resulting in poor yields (Fig. S1†), while in medium containing 1% FBS, the spheroids showed the better circularity and roundness and the minimal aspect ratio compared to those cultured with the 10% FBS condition (Fig. 2F). Therefore, among the three FBS concentrations, we selected the medium with 1% FBS to ensure proper spheroid formation and nutrient supply. After 8 days of culture of GBM spheroids, we seeded additional HUVECs labeled with blue cell tracker to generate the capillary model. After 14 days of co-culturing following HUVEC seeding, the HUVEC layer was formed around the core spheroid (Fig. 2G).

3.3. Cancer–artery model spheroid formation and their shape analysis

Arteries are characterized by muscle cells surrounding the blood vessels, so we hypothesized that artery models could

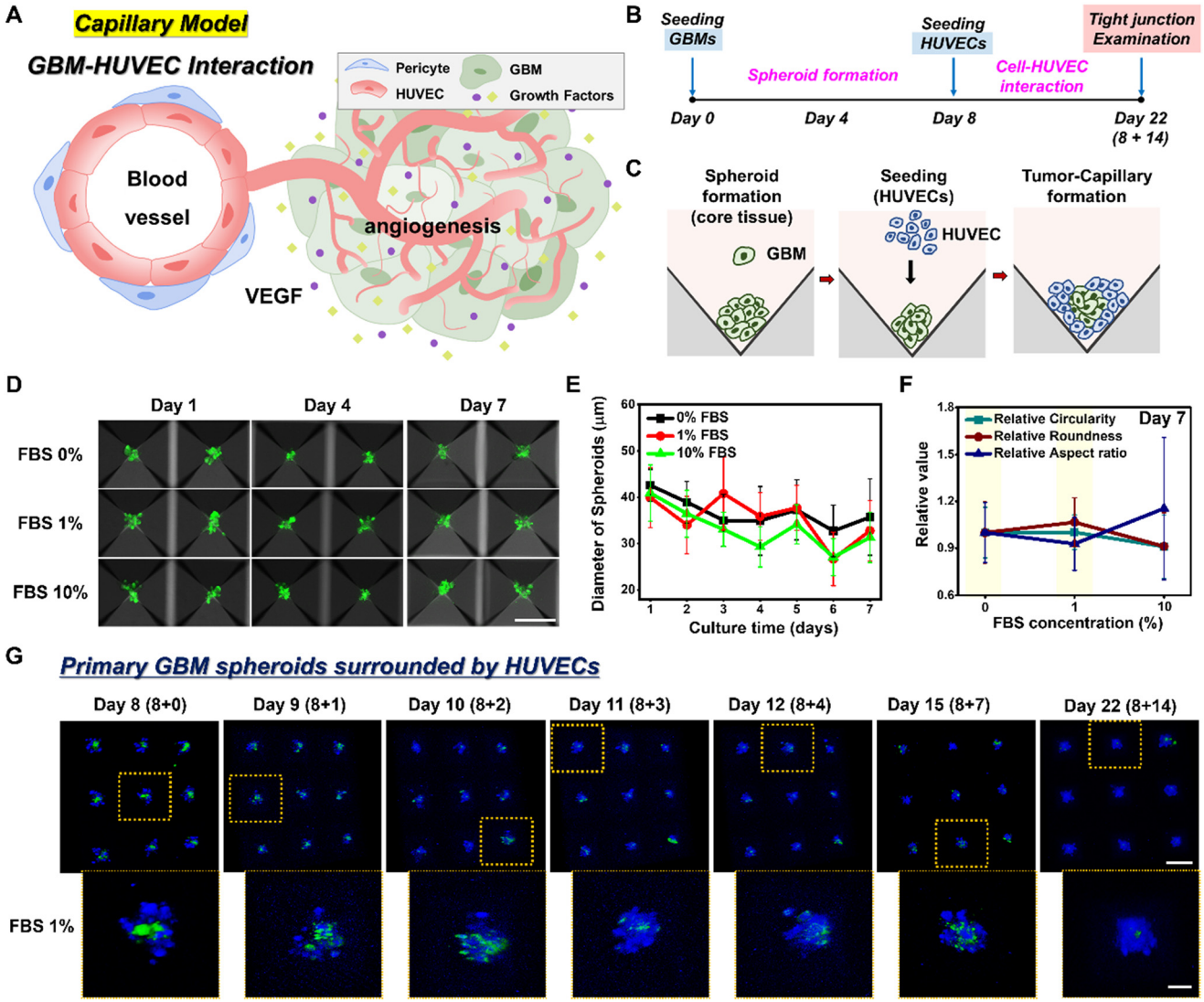

Fig. 2 Capillary model fabrication strategy. (A) Schematic of capillary angiogenic environment. (B) Timepoint of capillary model fabrication. (C) Illustration of the capillary (HUVEC) layer fabrication process. (D) Representative confocal 2D images of GBM spheroids days 1, 4, and 7 by FBS concentration. Scale bar: 200 μm. (E) Comparison of diameters by FBS concentration according to culture time. (F) Comparison of spheroid shape changes by FBS concentration on day 7. For the analysis of quantitative data, we analyzed at least 90 spheroids. (G) Representative confocal 2D images (top), 3D images of spheroids (bottom). Scale bars: 200 μm (top), 50 μm (bottom). Error bars represent s.d.

be easily made by adding a layer of SMCs between the tumor spheroids and HUVEC layer (Fig. 3A). To generate the artery model, we created core spheroids using GBM, added SMCs to form a muscle layer after 4 days, and then seeded HUVECs another 4 days later (Fig. 3B and C). GBMs, SMCs, and HUVECs were marked with green, red, and blue cell trackers, respectively, to show the formation of a multilayered spheroid (Fig. 3D and E). To ensure the quality of the core–shell structure, we examined cross-sections of the spheroid divided into top, middle, and bottom sections based on different heights (Fig. 3F and G). As expected, the top and bottom sections have a larger area for SMCs compared to GBMs, while the middle section has a relatively larger area for GBM (Fig. 3G). the findings showed that spheroids were effectively divided into a core and layers of SMCs and HUVECs, confirming the artery model formation mimicking the native tumor–artery interaction.

3.4. Effect of brain cancer cells on the properties of endothelial cells and expression of cell–cell junction markers

In general, tumors induce angiogenesis to obtain more nutrients and oxygen. For this reason, we first assumed that the presence of brain cancer cells might weaken the surrounding vascular cell layer and reduce the expression of junction markers compared to HUVEC only without tumors.[24] The expression levels of the adherens junction (VE-cadherin and PECAM) (Fig. 4A–C) and tight junction (occludin, and CLDN5) (Fig. 4D–F) markers on spheroids with capillary and artery layers were compared to HUVEC-

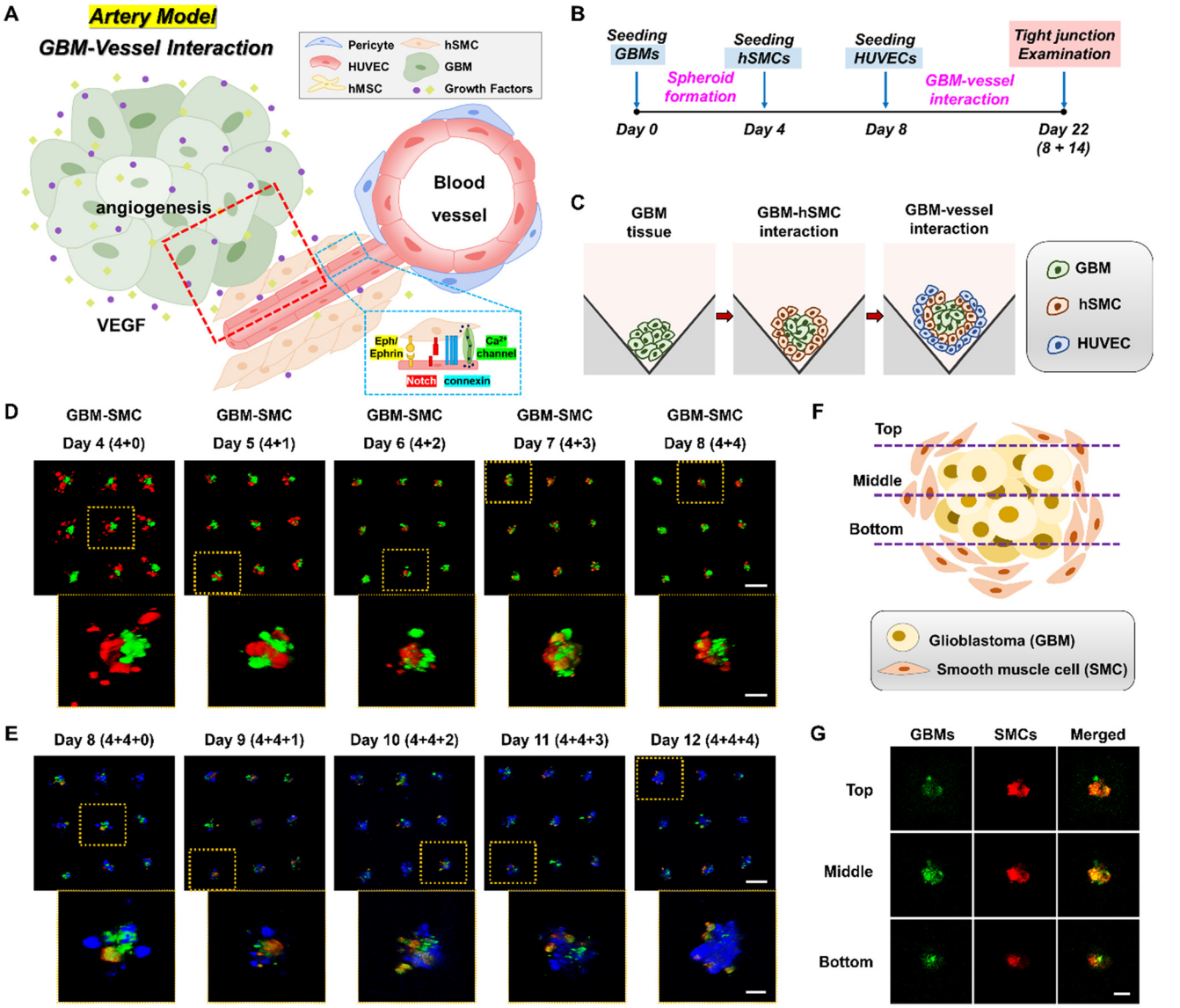

Fig. 3 Artery model fabrication strategy. (A) Schematic of artery angiogenic environment. (B) Timepoint of artery model fabrication. (C) Illustration of the artery (hSMC + HUVEC) layer fabrication process. (D) Representative confocal 3D image of the cancer–SMC layer formation process. Scale bars: 200 μm (top), 50 μm (bottom). (E) Representative confocal 3D image of the cancer spheroid–HUVEC layer formation process. Scale bars: 200 μm (top), 50 μm (bottom). (F) Illustration of spheroid section. (G) Representative confocal 3D images of cross-sectioned spheroids. Scale bar: 50 μm.

only spheroids without tumors. All quantification data for marker expression levels were divided by the mean value of the GBM spheroid (Fig. S2†) to compare HUVEC-specific marker expression levels in each model (Fig. 4B, C, E and F). In the case of VE-cadherin, occludin, and CLDN5, expression was decreased in capillary and artery models compared to HUVEC-only spheroids. Marker expression was weaker in capillary models than in artery models, which could be interpreted as SMC–HUVEC interactions present in artery models contributing to more stable vessel formation. Interestingly, in contrast, PECAM showed the opposite result; expression levels from both capillary and artery models were higher in the presence of brain cancer than in the condition of HUVEC-only spheroids (capillary model: ~2.2-fold, artery model: ~1.4-fold relative to HUVEC spheroid). To further analyze the gene expression of tumor/cap with or without vascular endothelial cells, we analyzed mRNA expression using real-time PCR technique (Fig. 4G and Table S1†). The experimental groups were GBM and capillary model (Cap; GBM + HUVEC), which were cultured for 22 days after forming spheroids. Comparing the mRNA expression of GBM and capillary model groups, most oncogenes (*BRAF*, *HER2*, *HER3*, *AKT*, *PI3K*), Rho signaling pathway (*CDC42*, *RAC1*), and metastasis-related genes (*CXCR4*) were upregulated in the GBM compared to the capillary model group. On the other hand, some of the oncogenes such as *KRAS*, *BRCA2*, and *MMP3* were observed in the capillary model group compared to GBM. Quantitative analysis showed that *BRAF*, *HER2*,

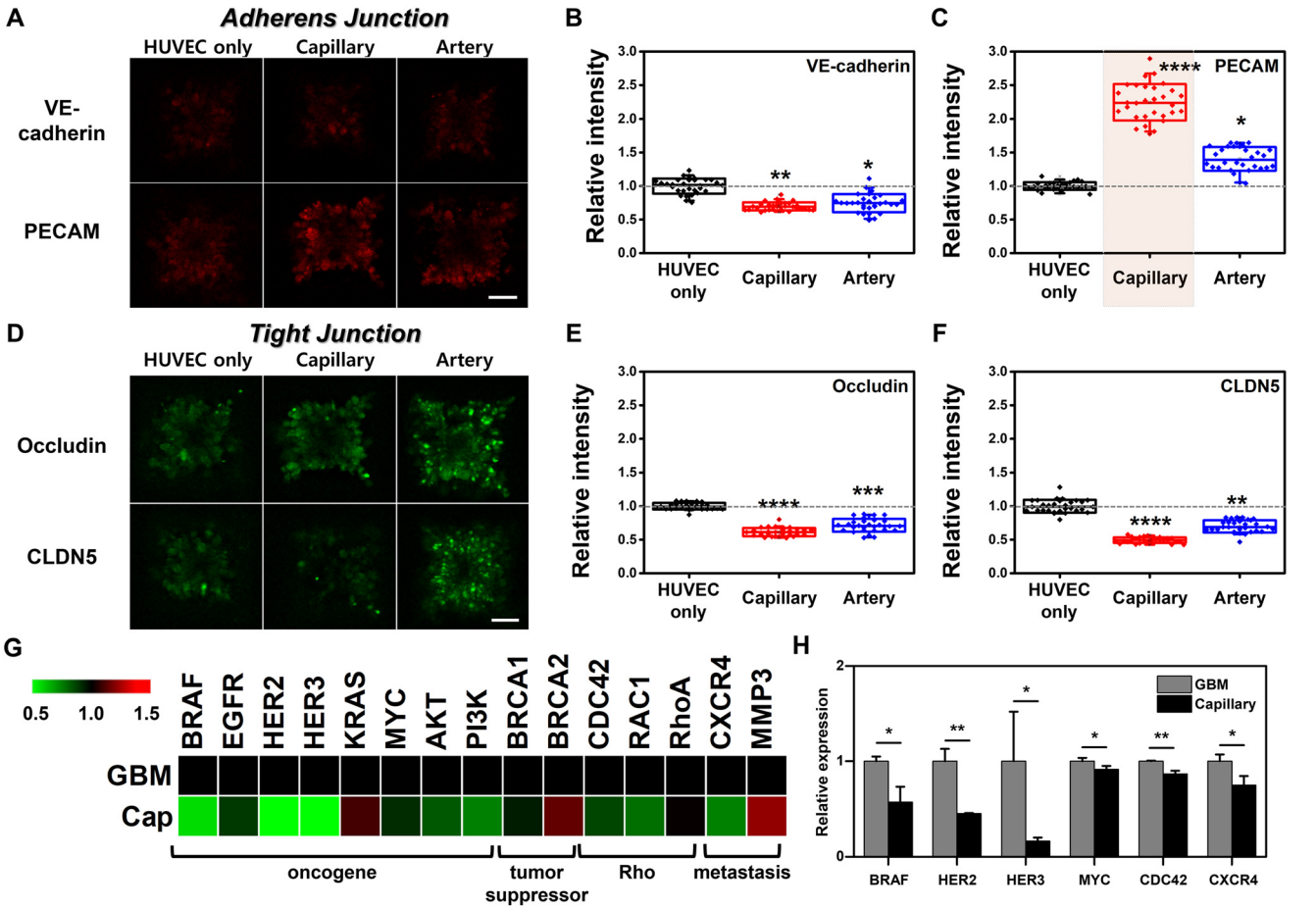

Fig. 4 PECAM is strongly expressed among junction markers resulting from GBM–HUVEC interaction. (A) Representative confocal images of adherens junction in spheroids. (B and C) Relative expression levels of VE-cadherin (B) and PECAM (C). (D) Representative confocal images of tight junction in spheroids. (E and F) Relative expression levels of occludin (E) and CLDN5 (F). All data in (B–F) were divided by the marker expression for each GBM only spheroids to remove values that are detected in cancer, and then normalized by the intensity value for HUVEC only spheroids. For the analysis of junction marker expression data, we analyzed at least 30 spheroids. (G) The heatmap chart of gene expression in GBM and the capillary model as determined by qRT-PCR. (H) Quantification of selected genes that are downregulated in capillary model (*$P < 0.05$, **$P < 0.01$, ***$P < 0.001$, ****$P < 0.0001$). Error bars represent standard deviation. Scale bar: 50 μm.

HER3, *MYC*, *CDC42*, *CXCR4* were ~1.8-, ~2.2-, ~6.1-, ~1.1-, ~1.2-, ~1.3-fold upregulated in GBM compared to capillary model group, respectively (Fig. 4H). These results suggest that the addition of vascular endothelial cells may alter the growth pattern of GBM. In particular, the presence of vascular endothelial cells may alter the microenvironment of GBM cells, reducing the environmental stress of the tumor cells and thus reducing the expression of oncogenes in tumor cells that are targeted for "proliferation". On the other hand, the interaction between GBM cells and vascular endothelial cells may influence the cells to focus more on MMP3-driven surrounding tissue invasion and metastasis rather than migration (CXCR3) or growth (oncogene).

When connecting PCR data with the role of PECAM in vascular endothelial cells, vascular endothelial cells with increased PECAM-1 expression may provide cellular signals to tumor cells, resulting in a phenotype shift from proliferation to invasion/metastasis. Taken together, these results provide that the presence of vascular endothelial cells can alter tumor proliferation/metastasis through various microenvironmental changes and interactions with tumor cells compared to GBM alone.

3.5. Differential interactions of various tumor types with HUVECs

We decided to apply the results from the capillary and artery models based on brain tumors to other types of tumors. By using patient-derived cancer cells, we expected to be able to observe their interactions with vascular cells while maintaining their unique tissue characteristics. After creating spheroids of various tissues using patient-derived cancer cells, junction marker analysis was performed (Fig. 5A and B). To obtain junction marker values expressed in HUVECs by interaction with cancer cells, rather than values expressed in cancer itself, junction markers were divided by the cancer-only spheroid values (Fig. S3†) and compared to the brain (Fig. 5C and D and S4†). The spheroid

shape and marker expression were different depending on the tissue origin. The different expression values of markers compared to brain suggest that each cancer tissue interacts differently with HUVECs. Since the PECAM expression in previous GMB only spheroids was interesting, we focused on the PECAM in this experiment (Fig. 5C and D). Compared to the PECAM expression of brain, liver and pancreas cancer expressed significantly low levels (~0.6- and ~0.6-fold at artery model, ~0.7- and ~0.6-fold at capillary model) while breast and lung cancer showed similar levels (~1.1- and ~1.2-fold at artery model, ~0.9- and ~0.7-fold at capillary model). We narrowed down the conditions to pancreas and lung by selecting one from the low expression group and one from the similar expression group. The pancreas and lung are suitable as PECAM comparison groups because they show similar trends in the expression of other junction markers compared to the brain. We used a cytokine array to indirectly determine how PECAM was highly expressed in the presence of brain cancer (Fig. S5 and Table S2†). By comparing the brain model to HUVEC only spheroids, pancreatic-capillary model, and lung-capillary model, we were able to determine whether there were any differences in cell secretion in the presence of brain cancer (Fig. 5E). Among these, we noted expression levels of interleukin 6 (IL-6), interleukin 8 (IL-8), macrophage migration inhibitory factor (MIF), and endothelial plasminogen activator inhibitor (Serpin E1) (Fig. 5F). All these proteins were strongly expressed in tumor–capillary model than in HUVEC only spheroids, with all four showing high expression levels in the brain cancer model (Fig. 5F).

The expression of these proteins was similar to the expression pattern of PECAM, which is overexpressed in tumor cell models compared to models containing only HUVECs. Notably, MIF, which is involved in immune regulation and inflammation, increases PECAM expression in vascular endothelial cells, which is known to regulate vasoconstriction and neutrophil migration in the tumor microenvironment.[25]

3.6. Evaluation of drug efficacy using a tumor spheroid model with vascular cell integration

We conducted drug efficacy validation to assess the applicability of the tumor spheroid-based model as a drug

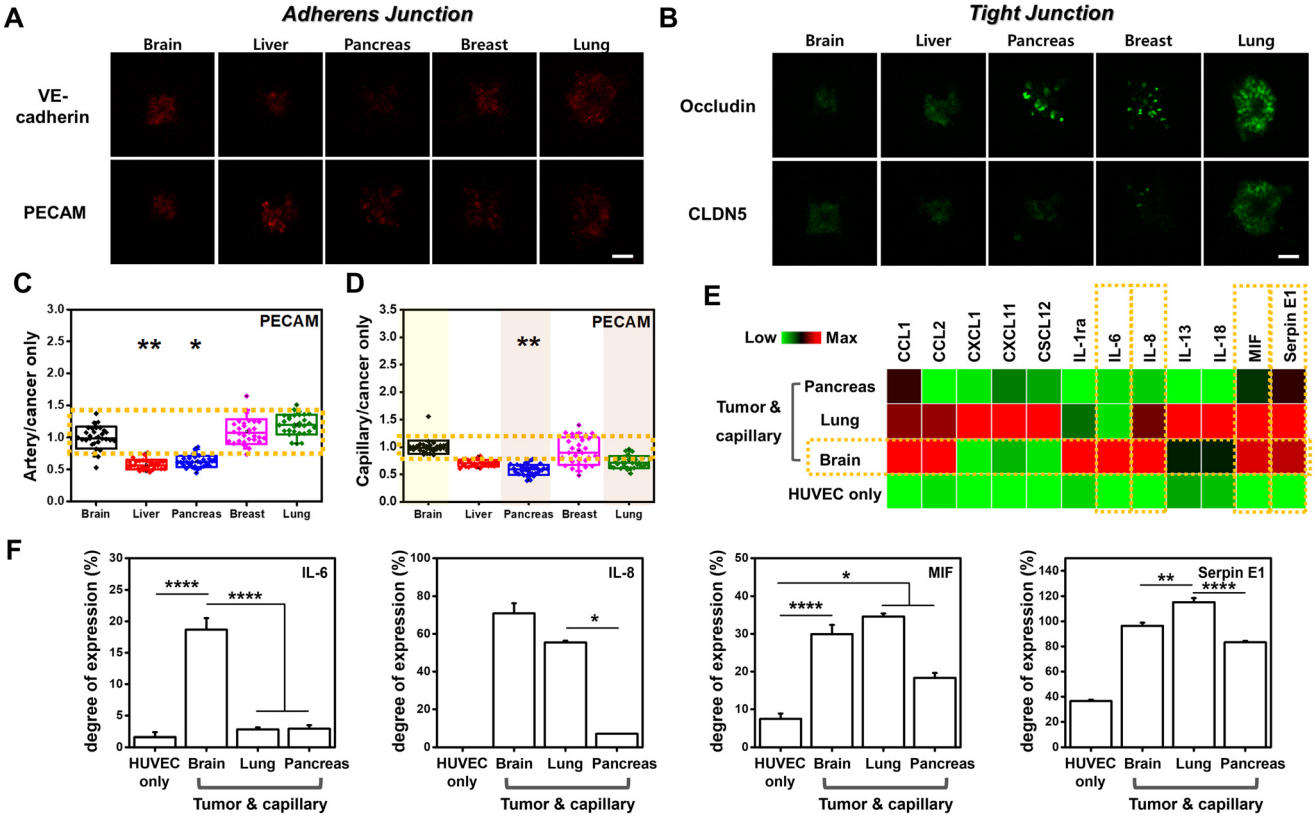

Fig. 5 Comparison with other cancer types shows that PECAM is highly expressed in brain cancer. (A) Representative confocal images of adherens junctions in spheroids derived from cancer cells of each organ. (B) Representative confocal images of tight junctions in spheroids derived from cancer cells of each organ. (C) Relative expression levels of PECAM in artery models. (D) Relative expression levels of PECAM in capillary models. All data in (C and D) were divided by the marker expression for each cancer only spheroids to remove values that are detected in cancer, and then normalized by the intensity value for brain cancer models. For the analysis of junction marker expression data, we analyzed at least 30 spheroids. (E) Heatmap of relative expression levels of human cytokine of capillary model by cancer type. The data was normalized by HUVEC only. (F) Compare expression of selected proteins that are strongly expressed in the brain (*$P < 0.05$, **$P < 0.01$, ***$P < 0.001$, ****$P < 0.0001$). Error bars represent standard deviation. Scale bar: 50 μm.

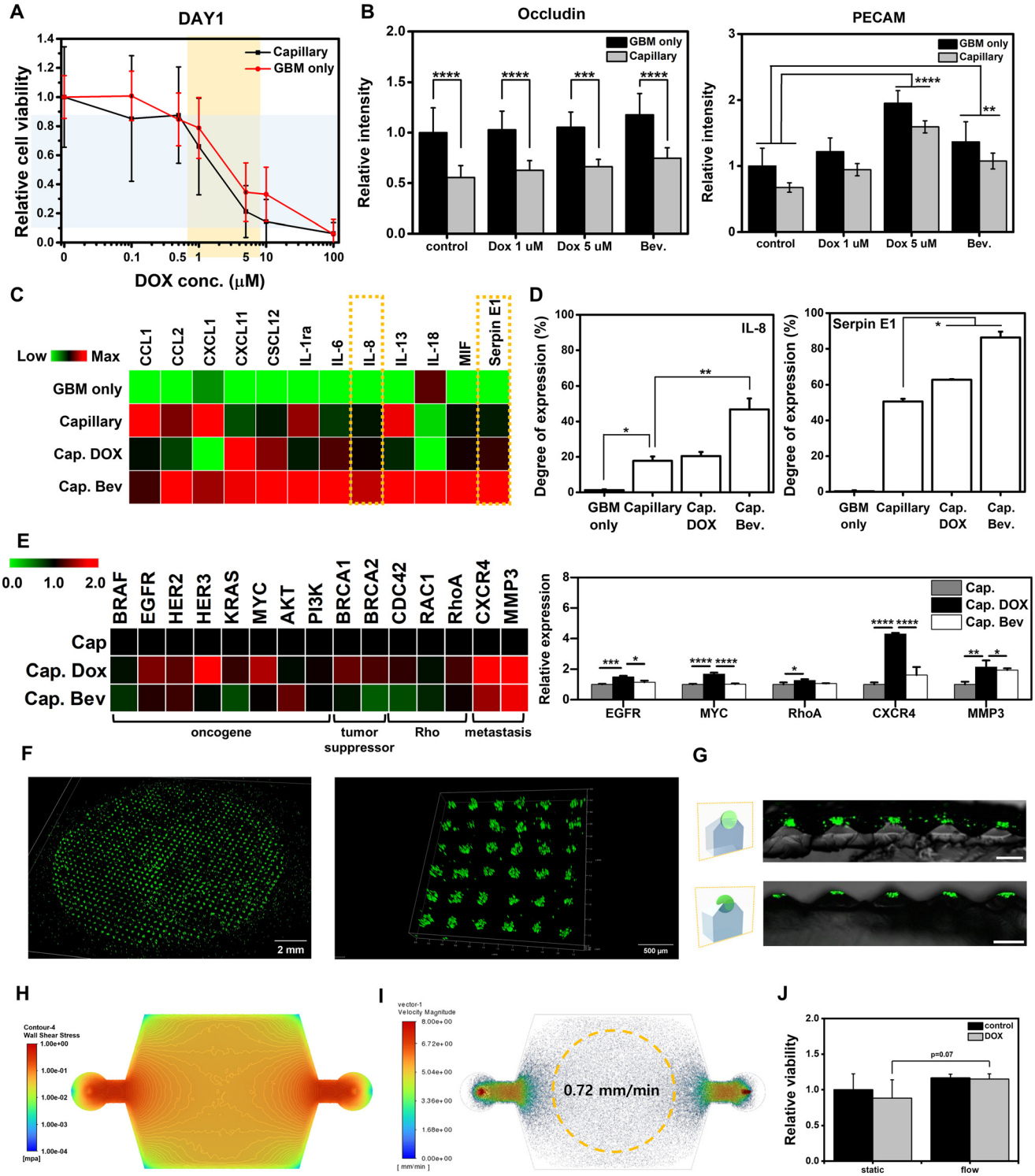

Fig. 6 Drug treatment in capillary models. (A) Relative spheroid viability of capillary and GBM only model by drug concentration. (B) Relative expression levels of occludin and PECAM in capillary and GBM only model by drug concentration. (C) Heatmap of relative expression levels of human cytokine by drug treatment. All data was normalized by GBM only. For the analysis of viability and junction marker expression data, we analyzed at least 30 spheroids. (D) The degree of expression of selectively highly expressed proteins in drug-treated conditions. (E) qRT-PCR data by drug treatment. (F) Representative confocal images of HTS platform. (G) Cross-sectioned image of HTS platform. Top: A cross-section through the center of a spheroid. Bottom: A cross-section along a position approximately one-half from the center. Scale bars: 200 μm. (H and I) Simulation of the wall shear stress (H) and velocity (I) of the fluidic device. (J) Relative viability of static and flow conditions in the presence of DOX. Data was normalized by control static condition (*$P < 0.05$, **$P < 0.01$, ***$P < 0.001$, ****$P < 0.0001$). Error bars represent standard deviation.

screening platform. We used an anticancer drug, doxorubicin (DOX), a chemotherapeutic agent widely used in the treatment of various cancers. The drug was administered on day 22, after model formation was complete. One day after administration, the efficacy of the drug was verified (Fig. S6†). To optimize the appropriate drug concentration for the assay, we investigated the viability of GBM spheroids and GBM–capillary model spheroids under various drug conditions (Fig. 6A). At concentrations of 1 μM to 5 μM, the viability of the spheroids decreased rapidly, but not all cells died. Therefore, we chose 1 μM and 5 μM as the concentration of drug to use in our experiment. Viability of the capillary models was generally lower than GBM only models, indicating that the viability of the cancer was lower in the presence of a endothelial cell layer (*e.g.*, ~0.66-fold at capillary model and ~0.78-fold at GBM only model for 5 μM DOX concentration). Anticancer drugs are administered to patients *via* intravenous injection rather than directly into the tumor. Thus, the capillary model offers a more physiologically relevant environment than cancer only model, as drug reaches the cancer cells through the vascular endothelial cells. To determine how changes in the cancer cells under the action of anticancer drugs affect the surrounding blood vessels, we compared occludin and PECAM marker expression (Fig. 6B). Additionally, we used bevacizumab (Bev), a drug that targets VEGF in vascular endothelial cells to block angiogenesis, to explore differences in drug mechanisms. Bev was used at a concentration of 168 nM based on previous studies.[16,26] Occludin expression showed significant difference between the GBM only and capillary models, but differences by drug concentration or type were not significant. In contrast, PECAM showed stronger expression with increasing drug concentration in both GBM only and capillary models. Increased expression of PECAM in the presence of Bev was also significant. This could be interpreted as PECAM being more sensitive to drug-induced changes in cancer cells, even though the two drugs used had different mechanisms of action, supporting previous our hypotheses that PECAM plays an important role in the relationship between cancer cells and the surrounding HUVECs. To ascertain the alterations in protein secretion that occurred after anticancer drug treatment were associated with decreased survival and additional PECAM changes, a cytokine array was performed (Fig. 6C). The secreted proteins were different in the presence and absence of vascular cells (Fig. S7A†). There were significant differences in the secretion of IL-8, serpin E1, and MIF proteins, which are involved in angiogenesis and cancer growth.[27,28] They showed increased expression in the anticancer drug treated group, with stronger expression in the Bev treated group (Fig. 6D and S7B†). This was interpreted to be due to compensatory mechanisms to maintain angiogenesis and cancer growth.[29–31]

To determine the changes in mRNA expression levels of GBM and capillary model in response to two anticancer drugs (DOX and Bev), qRT-PCR was performed and the changes in genes were analyzed by heatmap chart (Fig. 6E and S8†). The results showed that all DOX treated groups (GBM–DOX, Cap–DOX) showed upregulation of oncogene such as *EGFR*, *MYC*, and *CXCR4*, *MMP3*, which are related to metastasis. Interestingly, the GBM–DOX showed downregulation of *BRAF*, *HER2*, and *AKT* among oncogenes compared to the GBM only, while the Cap–DOX showed upregulation of *HER2* and *HER3* compared to the Cap only (without drug). On the other hand, the difference in gene expression between GBM–Bev and Cap–Bev was more significant. In the GBM–Bev group, significant downregulation of oncogene *BRAF*, *HER2*, *HER3*, *KRAS*, Rho signaling, and upregulation of metastasis-related genes (*MMP3*) were observed, while in the Cap–Bev group, no significant gene expression changes were observed other than upregulation of metastasis-related genes (*CXCR4*, *MMP3*). Quantitative analysis showed that *EGFR*, *MYC*, and *RhoA*, *CXCR4*, *MMP3* were ~1.5-, ~1.7-, ~4.3, ~2.1, ~1.3-fold upregulated in Cap–DOX compared to Cap only, respectively. On the other hand, Cap–Bev increased only CXCR4 and MMP3, genes associated with metastasis, by ~1.6 and ~1.9-fold compared to Cap only, respectively, while no statistical significance was observed for other genes.

The responsiveness of gene expression to these drugs can be considered to represent the difference between GBM and Cap groups. In the GBM group, apoptosis and stress response are strongly induced by DOX, resulting in changes in the expression of oncogene, *etc.*, whereas in the Cap group, the presence of vascular endothelial cells may moderate the fluctuations in the expression of genes or promote complementary responses. These results may indicate that vascular endothelial cells interact with tumor cells to exert a compounding effect on tumor growth and metastasis. Therefore, the presence of HUVECs may be indispensable when modeling tumors and analyzing their drug responsiveness.

In addition, the differences in gene expression (oncogene expression) between the Cap–DOX and Cap–Bev groups are thought to reflect differences in the mechanisms of action of each anticancer drug. In the case of DOX, tumor cells at sublethal doses are strongly induced to undergo an intracellular stress response due to its incorporation into the DNA of tumor cells, which can activate signaling pathways for cell survival. In addition, as tumor cells attempt to compensate for the damage caused by DOX, oncogene activation may occur to counteract the DNA damage. On the other hand, in the case of Bev, the expression of oncogene for survival does not seem to be increased because it is an anticancer drug whose main mechanism is inhibition of angiogenesis by inhibiting VEGF, which inhibits angiogenesis for tumor growth rather than directly damaging tumor cells and inducing intracellular stress responses. In addition, the increase in metastasis-related genes with the use of both anticancer drugs suggests that the use of both anticancer drugs helps to kill tumor cells but may change the phenotype of tumor cells to a form that favors "metastasis". Our results indicate that our capillary model can predict drug-induced underlying tumoral responses as well as biological phenomena that may be observed in the native tumor/vascular crosstalk.

The decreased cell viability and altered secretion of cytokines after drug treatment, as in patients, means that our model simulates the native cancer capillary environment well. Therefore, we developed this spheroid-based model into a high-throughput drug screening model by adapting it to the HTS platform and introducing a flow device. We performed DOX drug testing in HTS platform in both flow and static environments. HTS platform was made by stamping out spheroids using GelMA as described previously (Fig. 1C). Almost all pre-made spheroid models were moved to HTS platform (Fig. 6F, Videos S1 and S2†). The cross-sectional image confirmed that the spheroids in microwells were not embedded in the gel (Fig. 6G). Therefore, the models could sense the shear stress directly from the flow. The device was designed to have a single HTS platform and uniform shear stress across all areas (Fig. S9A†). The distribution of shear stress (Fig. 6H) and fluid velocity (Fig. 6I) in the system appeared under gravity-driven flow conditions. The simulation data demonstrated that within the HTS platform range, the average velocity was 0.72 mm min^{-1} and the average wall shear stress was 4.85×10^{-2} mPa. The distribution of pressure was also simulated; its average value was 7.13 mPa within sample range (Fig. S9B†). Moreover, the above three physical quantities remained nearly constant within the HTS platform range (Fig. S9C–E†). These results were utilized to design a device with appropriate parameters to regulate flow velocity within physiological ranges of shear rates. Viability was low in the presence of the anticancer drug in both static and flow environments (Fig. 6J). It was observed that in the presence of flow, viability increased for both the control and drug-treated groups (*e.g.*, ~1.16-fold at control model and ~1.3-fold at drug model at flow concentration). This is because the flowing fluid stimulates shear, which provides an environment that more closely resembles the native model and helps cells survive.[32,33]

3.7. A comparative study of MSCs and SMCs in cancer–endothelial cell interactions

We decided to investigate how other vascular neighbors interact with HUVECs. It is well-known that differentiated MSCs into pericytes reside around blood vessels.[34,35] Pericytes play a crucial role in the formation, maintenance, and regulation of blood vessels. We expanded our research on arteries and capillaries by comparing how MSCs and SMCs affect cancer–HUVEC interactions (Fig. 7A). We found that both MSC–HUVEC and SMC–HUVEC spheroids were similar in size and shape in the 1% FBS condition, of which condition was chosen in our previous GBM–HUVEC experiments (Fig. 7B and C). MSCs and SMCs were placed on the core in the same way as the capillary model and grown for 7 days. The HUVECs layer was then created and given 14 days of spheroid formation time (Fig. 7D and E). To see the changes of HUVECs according to the core cells, we performed junction marker evaluation. With VE-cadherin evaluation, both MSCs and SMCs showed similar marker expression (Fig. 7F). In addition, both MSCs and SMCs showed a slight increase in PECAM, but the difference was not significant (Fig. 7G). In tight junction marker analysis using occludin and CLDN5, MSCs showed a significant increase level of their expression (Fig. 7H and I). In contrast, SMCs showed slightly increased expression, but the difference was not significant. Taken together, MSCs and SMCs, as vascular-neighbor cells, directly interact with HUVECs to strengthen the junctions of HUVECs, with MSCs contributing more to junctional strengthening than SMCs. PECAM expression was higher in the capillary model without SMCs compared to HUVEC-only and artery model (Fig. 4C). Direct contact of GBM secreted material with HUVECs was likely the dominant influence on the elevated PECAM expression in the capillary model. From the previous results, we speculate that within the GBM artery model, SMCs may have played a role in disrupting the direct interaction between GBM and HUVECs rather than enhancing junction formation and maturation of HUVECs.

4. Conclusion

In this study, we created a tumor–endothelial cell spheroid model within blood vessel spheroid model that can be used for high-throughput screening of cancer-targeting drugs. The spheroid model was an inverted version of the actual human body, with a cancer core spheroid surrounded by an endothelial cell layer and a muscle layer in the case of arteries. Observation of junction proteins using the spheroid model revealed strong expression of PECAM in the presence of cancer cells, especially in the interaction of GBM and HUVECs. Through junctional and cytokine comparisons with cancer cells derived from liver, pancreas, breast, and lung, we confirmed that the strong expression of PECAM was observed for GBM-based models. The mRNA expression level analysis showed that the presence of HUVECs with GBM could affect the phenotype of tumor cells to switch from growth to metastasis. Drug testing was performed using DOX and Bev; when evaluating junction markers under viability conditions, we found that the expression of PECAM increased as the drug concentration increased. After drug treatment, the secretion of cytokines involved in drug resistance increased, and among the increased cytokines were proteins involved in PECAM expression. Through mRNA expression level analysis, we found that the phenotype of tumor cells was complementarily altered upon treatment with DOX (acting directly on tumor cells) and Bev (inhibiting-angiogenesis) in terms of responsiveness to anticancer drugs with different anticancer mechanisms. Correlating the PCR data with the cytokine data once again confirmed the role of PECAM in the correlation between blood vessels and tumors. Viability was increased in the drug environment with flow compared to static conditions, indicating that an environment similar to the nature environment including shear stress and mass exchange might be created. Although HUVECs do not

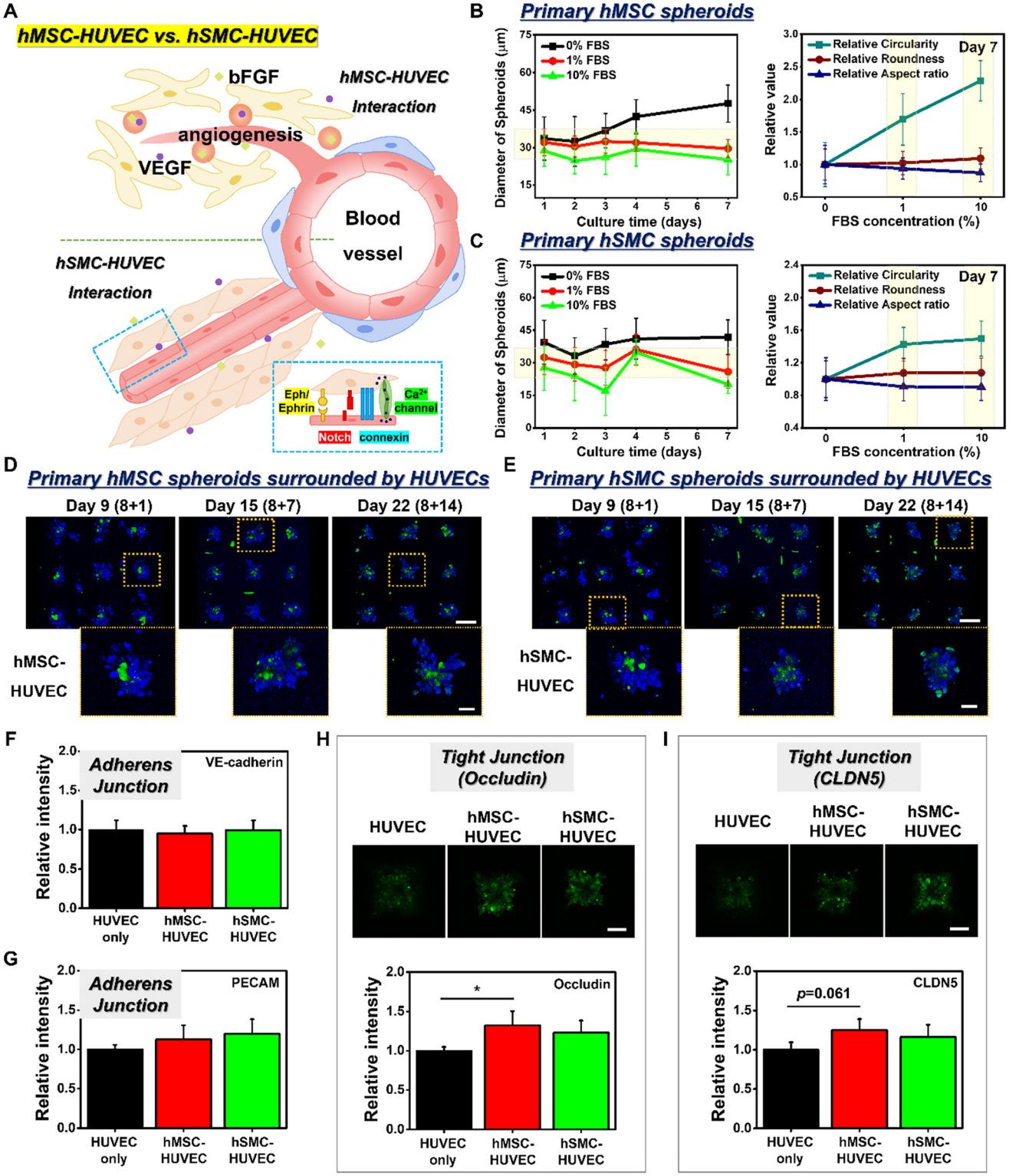

Fig. 7 Comparison of interactions between vascular peripheral cells and endothelial cells. (A) Schematic of MSCs and SMCs interaction with vessel. (B) Comparison of MSCs spheroid size and shape by FBS concentration. (C) Comparison of SMCs spheroid size and shape by FBS concentration. For the analysis of quantitative data, we analyzed at least 90 spheroids. (D) Representative confocal 3D image of the MSC spheroid–HUVEC layer formation process. (E) Representative confocal 3D image of the SMC spheroid–HUVEC layer formation process. Scale bar: 200 μm (top), 50 μm (bottom). (F) Relative expression levels of VE-cadherin. (G) Relative expression levels of PECAM. (H) Representative confocal 2D image of occludin and relative expression levels. (I) Representative confocal 2D image of CLDN5 and relative expression levels. All data in (F–I) were normalized by the intensity value for HUVEC only spheroids (*$P < 0.05$). Error bars represent standard deviation. For the analysis of junction marker expression data, we analyzed at least 30 spheroids. Scale bar: 50 μm.

completely surround the core spheroid, they form a layer that provides sufficient insight into interactions based on different tumor types and vascular model types, supporting the design of cancer treatment models for efficient delivery of tumor-targeting drugs across blood–tumor barriers.

Since we focused on the direct interaction between the cancer layer and the endothelial cell layer of the spheroid, we acknowledged that the lumen structure resulting from the interaction with the external vessel was not confirmed. However, by providing an environment where direct interaction between cancer cells and vascular cells was possible, it was closer to biomimicry and can provide a deeper exploration of the interaction between cancer and vascular cells. In addition, since most anti-cancer drugs are injected intravenously, this model of the interaction between cancer and vascular endothelial cells could be used for effective drug screening. Although it has limitations for advanced drug screening without lumen formation, it is valuable for demonstrating drug responses at the cancer-cell and endothelial-interface level. Furthermore, it was easy to make large amounts of uniform spheroids, which indicates that it could be applied as a high-throughput drug screening model. Our model provides valuable insights into vascular cell interactions and can be applied to study vascular diseases such as vascular remodeling and atherosclerosis. Additionally, it can be adapted to investigate tissue-specific interactions with blood vessels in contexts like inflammation and regenerative medicine. This flexibility extends the model's potential applications to a variety of vascular-related diseases and tissue studies.

Data availability

The data supporting the findings of this study are available upon reasonable request. Interested parties should contact the corresponding author at junmin@postech.ac.kr.

Conflicts of interest

There are no conflicts to declare.

Acknowledgements

We gratefully acknowledge funding from National Research Foundation of Korea (NRF) grant (RS-2023-00211096, RS-2023-00260454, and RS-2024-00403376) funded by the Korean Government (MSIT) as well as Glocal University 30 Projects (Biomedical Engineering Center). This research was also supported by the Korea University grant (K2419141). Authors also thank Prof. Seung Soo Oh at POSTECH MSE for help with confocal imaging.

References

1 V. L. Bautch and K. M. Caron, Blood and lymphatic vessel formation, *Cold Spring Harbor Perspect. Biol.*, 2015, **7**(3), a008268.
2 N. M. Anderson and M. C. Simon, The tumor microenvironment, *Curr. Biol.*, 2020, **30**(16), R921–R925.
3 K. Tei, N. Kawakami-Kimura, O. Taguchi, K. Kumamoto, S. Higashiyama and N. Taniguchi, *et al.*, Roles of cell adhesion molecules in tumor angiogenesis induced by cotransplantation of cancer and endothelial cells to nude rats, *Cancer Res.*, 2002, **62**(21), 6289–6296.
4 O. Van Tellingen, B. Yetkin-Arik, M. De Gooijer, P. Wesseling, T. Wurdinger and H. De Vries, Overcoming the blood–brain tumor barrier for effective glioblastoma treatment, *Drug Resistance Updates*, 2015, **19**, 1–12.
5 C. D. Arvanitis, G. B. Ferraro and R. K. Jain, The blood–brain barrier and blood–tumour barrier in brain tumours and metastases, *Nat. Rev. Cancer*, 2020, **20**(1), 26–41.
6 J. Cedervall, A. Dimberg and A.-K. Olsson, Tumor-induced local and systemic impact on blood vessel function, *Mediators Inflammation*, 2015, **2015**(1), 418290.
7 S. Kim, J. Ko, S.-R. Lee, D. Park, S. Park and N. L. Jeon, Anchor-IMPACT: A standardized microfluidic platform for high-throughput antiangiogenic drug screening, *Biotechnol. Bioeng.*, 2021, **118**(7), 2524–2535.
8 S. Lee, H. Kang, D. Park, J. Yu, S. K. Koh and D. Cho, *et al.*, Modeling 3D Human Tumor Lymphatic Vessel Network Using High-Throughput Platform, *Adv. Biol.*, 2021, **5**(2), 2000195.
9 Y. Fan, D. T. Nguyen, Y. Akay, F. Xu and M. Akay, Engineering a Brain Cancer Chip for High-throughput Drug Screening, *Sci. Rep.*, 2016, **6**(1), 25062.
10 N. Rahimi, Defenders and challengers of endothelial barrier function, *Front. Immunol.*, 2017, **8**, 1847.
11 J. Gavard and J. S. Gutkind, VE-cadherin and claudin-5: it takes two to tango, *Nat. Cell Biol.*, 2008, **10**(8), 883–885.
12 M. Hu, H. Zhang, Q. Liu and Q. Hao, Structural basis for human PECAM-1-mediated trans-homophilic cell adhesion, *Sci. Rep.*, 2016, **6**(1), 38655.
13 M. W. Dewhirst and T. W. Secomb, Transport of drugs from blood vessels to tumour tissue, *Nat. Rev. Cancer*, 2017, **17**(12), 738–750.
14 K. Sobierajska, W. M. Ciszewski, I. Sacewicz-Hofman and J. Niewiarowska, Endothelial cells in the tumor microenvironment, *Tumor microenvironment: Non-hematopoietic cells*, 2020, pp. 71–86.
15 G. Cao, C. D. O'Brien, Z. Zhou, S. M. Sanders, J. N. Greenbaum and A. Makrigiannakis, *et al.*, Involvement of human PECAM-1 in angiogenesis and in vitro endothelial cell migration, *Am. J. Physiol. Cell Physiol.*, 2002, **282**(5), C1181–C1190.
16 S. Tabasum, D. Thapa, A. Giobbie-Hurder, J. L. Weirather, M. Campisi and P. J. Schol, *et al.*, EDIL3 as an angiogenic target of immune exclusion following checkpoint blockade, *Cancer Immunol. Res.*, 2023, **11**(11), 1493–1507.
17 C. Poon, Measuring the density and viscosity of culture media for optimized computational fluid dynamics analysis of in vitro devices, *J. Mech. Behav. Biomed. Mater.*, 2022, **126**, 105024.

18 C. Quintard, E. Tubbs, G. Jonsson, J. Jiao, J. Wang and N. Werschler, *et al.*, A microfluidic platform integrating functional vascularized organoids-on-chip, *Nat. Commun.*, 2024, **15**(1), 1452.

19 J. Ko, S. Hyung, Y. J. Heo, S. Jung, S. T. Kim and S. H. Park, *et al.*, Patient-derived tumor spheroid-induced angiogenesis preclinical platform for exploring therapeutic vulnerabilities in cancer, *Biomaterials*, 2024, 122504.

20 D.-H. Choi, H.-W. Liu, Y. H. Jung, J. Ahn, J.-A. Kim and D. Oh, *et al.*, Analyzing angiogenesis on a chip using deep learning-based image processing, *Lab Chip*, 2023, **23**(3), 475–484.

21 M. G. Lampugnani, Endothelial cell-to-cell junctions: adhesion and signaling in physiology and pathology, *Cold Spring Harbor Perspect. Med.*, 2012, **2**(10), a006528.

22 S. G. Milton and V. P. Knutson, Comparison of the function of the tight junctions of endothelial cells and epithelial cells in regulating the movement of electrolytes and macromolecules across the cell monolayer, *J. Cell. Physiol.*, 1990, **144**(3), 498–504.

23 H. K. Campbell, J. L. Maiers and K. A. DeMali, Interplay between tight junctions & adherens junctions, *Exp. Cell Res.*, 2017, **358**(1), 39–44.

24 M. B. Schaaf, A. D. Garg and P. Agostinis, Defining the role of the tumor vasculature in antitumor immunity and immunotherapy, *Cell Death Dis.*, 2018, **9**(2), 115.

25 A. S. Pellowe, M. Sauler, Y. Hou, J. Merola, R. Liu, B. Calderon, H. M. Lauridsen, M. R. Harris, L. Leng and Y. Zhang, Endothelial cell-secreted MIF reduces pericyte contractility and enhances neutrophil extravasation, *FASEB J.*, 2019, **33**(2), 2171.

26 D. Klaver, H. Gander, G. Dobler, A. Rahm and M. Thurnher, The P2Y11 receptor of human M2 macrophages activates canonical and IL-1 receptor signaling to translate the extracellular danger signal ATP into anti-inflammatory and pro-angiogenic responses, *Cell. Mol. Life Sci.*, 2022, **79**(10), 519.

27 F. Seker, A. Cingoz, I. Sur-Erdem, N. Erguder, A. Erkent and F. Uyulur, *et al.*, Identification of SERPINE1 as a regulator of glioblastoma cell dispersal with transcriptome profiling, *Cancers*, 2019, **11**(11), 1651.

28 C. Qiao, S. Li, H. Lu, F. Meng, Y. Fan and Y. Guo, *et al.*, Laminar flow attenuates macrophage migration inhibitory factor expression in endothelial cells, *Sci. Rep.*, 2018, **8**(1), 2360.

29 H. Liu, Q. Zhao, L. Tan, X. Wu, R. Huang and Y. Zuo, *et al.*, Neutralizing IL-8 potentiates immune checkpoint blockade efficacy for glioma, *Cancer Cell*, 2023, **41**(4), 693–710, e8.

30 T. E. Kelly, C. L. Spillane, M. P. Ward, K. Hokamp, Y. Huang and P. Tewari, *et al.*, Plasminogen activator inhibitor 1 is associated with high-grade serous ovarian cancer metastasis and is reduced in patients who have received neoadjuvant chemotherapy, *Front. Cell Dev. Biol.*, 2023, **11**, 1150991.

31 L. Zhang, B. Ye, Z. Chen and Z.-S. Chen, Progress in the studies on the molecular mechanisms associated with multidrug resistance in cancers, *Acta Pharm. Sin. B*, 2023, **13**(3), 982–997.

32 A. Mishra, R. Kai, S. Atkuru, Y. Dai, F. Piccinini and P. M. Preshaw, *et al.*, Fluid flow-induced modulation of viability and osteodifferentiation of periodontal ligament stem cell spheroids-on-chip, *Biomater. Sci.*, 2023, **11**(22), 7432–7444.

33 B. Patra, C.-C. Peng, W.-H. Liao, C.-H. Lee and Y.-C. Tung, Drug testing and flow cytometry analysis on a large number of uniform sized tumor spheroids using a microfluidic device, *Sci. Rep.*, 2016, **6**(1), 21061.

34 G. Bergers and S. Song, The role of pericytes in blood-vessel formation and maintenance, *Neuro-Oncology*, 2005, **7**(4), 452–464.

35 L. S. Brown, C. G. Foster, J.-M. Courtney, N. E. King, D. W. Howells and B. A. Sutherland, Pericytes and neurovascular function in the healthy and diseased brain, *Front. Cell. Neurosci.*, 2019, **13**, 282.